Supporting information

Hydrate enabled the self-reconstruction of NiMoO$_4$ for efficient water oxidation

Jianmin Wang,[b,†] Hongyu Zhao, [b,†] Hao Zhang[b], Haitao Huang, [a,c,] Ruoyu Huang[b], Haijin Li,[a,b,*] Yongtao Li,[a,c,*] Xiaofang Liu, [b,*] Xiaolong Deng [a,d]

[a] Low-Carbon New Materials Research Center, Low-Carbon Research Institute, Anhui University of Technology, Ma'anshan, 243002, P. R. China

[b] School of Energy and Environment, Anhui University of Technology, Ma'anshan, 243002, P. R. China

[c] School of Materials Science and Engineering, Anhui University of Technology, Ma'anshan, 243002, P. R. China

[d] School of Microelectronics and Data Science, Anhui University of Technology, Ma'anshan, 243002, P. R. China

† Wang and Zhao equally contribute to the work.

[*] Corresponding Authors: Haijin Li, lihaijin@ahut.edu.cn; Yongtao Li, liyongtao@ahut.edu.cn; Xiaofang Liu, xfliu2003@163.com.
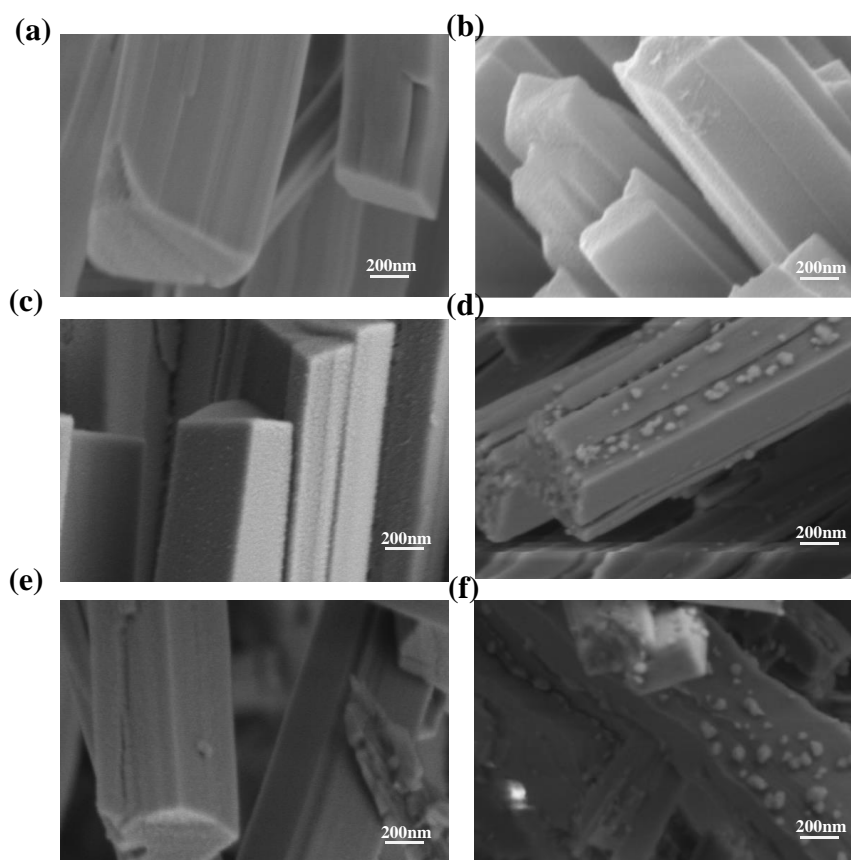
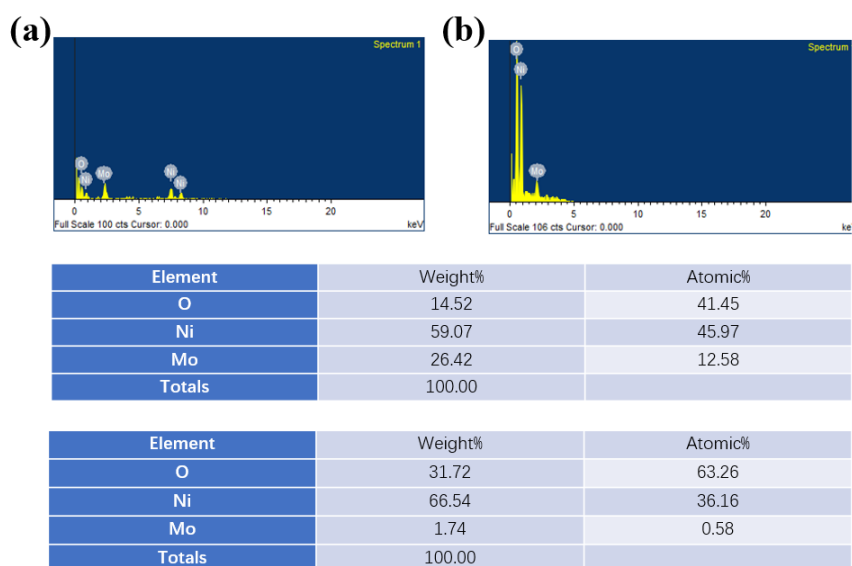Figure S1 SEM images of (a, b) NiMoO$_4$-350; (c, d) NiMoO$_4$-550; (e, f) NiMoO$_4$-650 before and after CV etching.

Element	Weight%	Atomic%
O	14.52	41.45
Ni	59.07	45.97
Mo	26.42	12.58
Totals	100.00	

Element	Weight%	Atomic%
O	31.72	63.26
Ni	66.54	36.16
Mo	1.74	0.58
Totals	100.00	

Figure S2 EDS spectrum of NiMoO$_4 \cdot$xH$_2$O (a) before CV; (b) after CV.

Element	Wt%	At%
O	13.49	41.43
Ni	43.85	36.71
Mo	42.67	21.86
Total	100.00	100.00

Element	Wt%	At%
O	7.39	25.00
Ni	63.70	58.70
Mo	28.91	16.30
Total	100.00	100.00

Element	Wt%	At%
O	27.01	58.02
Ni	69.71	40.81
Mo	3.28	1.17
Total	100.00	100.00

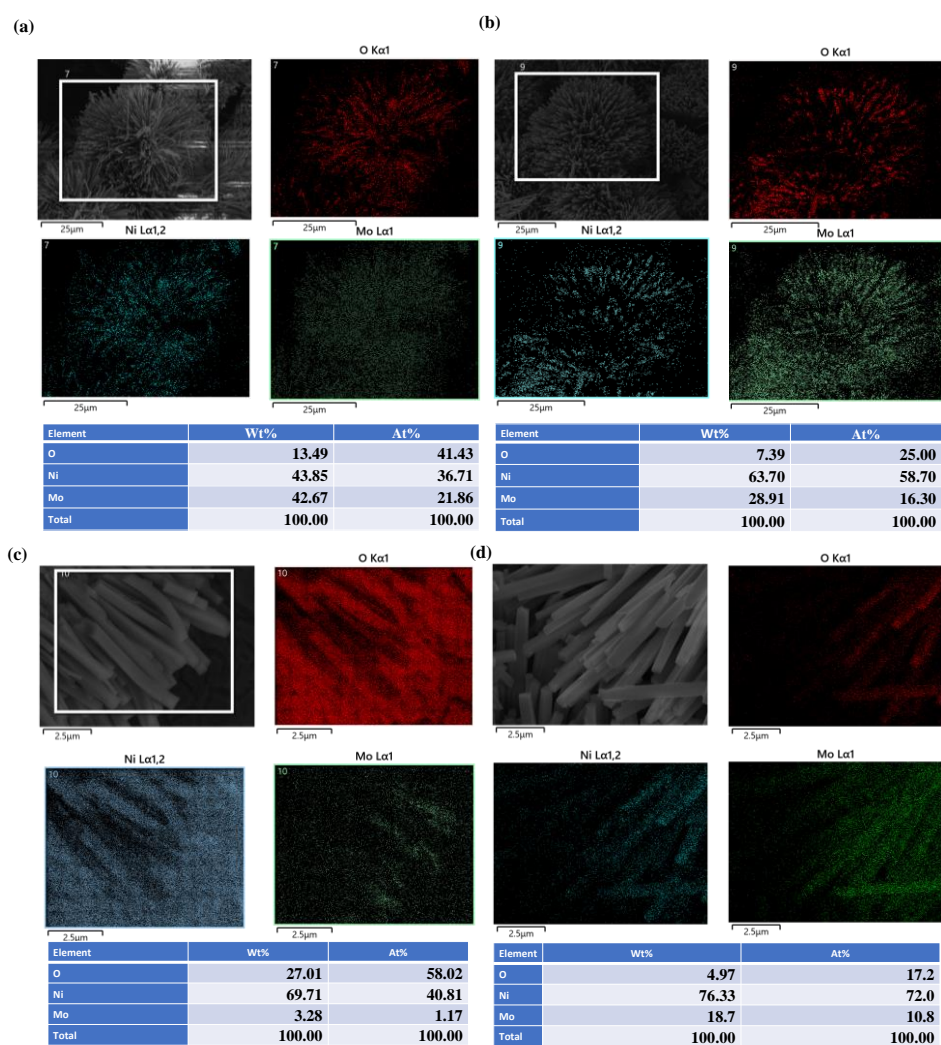| Element	Wt%	At%
O	4.97	17.2
Ni	76.33	72.0
Mo	18.7	10.8
Total	100.00	100.00

Figure S3 EDS spectrum of (a, b) NiMoO$_4$-550 before CV and after CV. (c, d) NiMoO$_4 \cdot$xH$_2$O and NiMoO$_4$-550 after long-time duration test at a current density of 100 mA cm^{-2}.

NiMoO$_4$-350

Element	Wt%	At%
O	24.13	60.63
Ni	28.48	19.50
Mo	47.40	19.86
Total	100.00	100.00

NiMoO$_4$-350-CV

Element	Wt%	At%
O	20.69	50.19
Ni	69.07	45.66
Mo	10.24	4.14
Total	100.00	100.00

NiMoO$_4$-650

Element	Wt%	At%
O	14.69	43.81
Ni	43.70	35.51
Mo	41.61	20.69
Total	100.00	100.00

NiMoO$_4$-650-CV

Element	Wt%	At%
O	22.49	58.06
Ni	31.43	22.11
Mo	46.08	19.83
Total	100.00	100.00

Figure S4 EDS spectrum of NiMoO$_4$-350 and NiMoO$_4$-650 before CV and after CV.
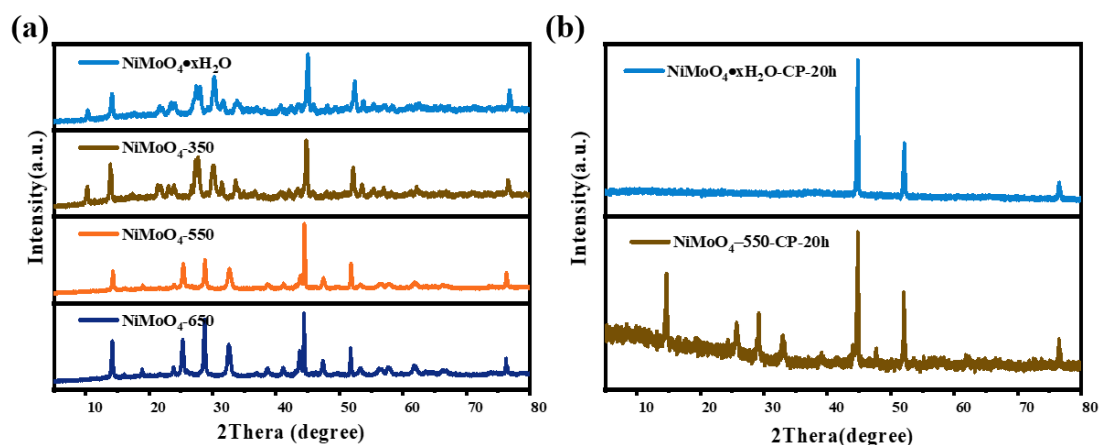
Figure S5 XRD patterns of (a)NiMoO$_4$•xH$_2$O, NiMoO$_4$-350, NiMoO$_4$-550 and NiMoO$_4$-650;(b) NiMoO$_4$•xH$_2$O-CP and NiMoO$_4$-550-CP.
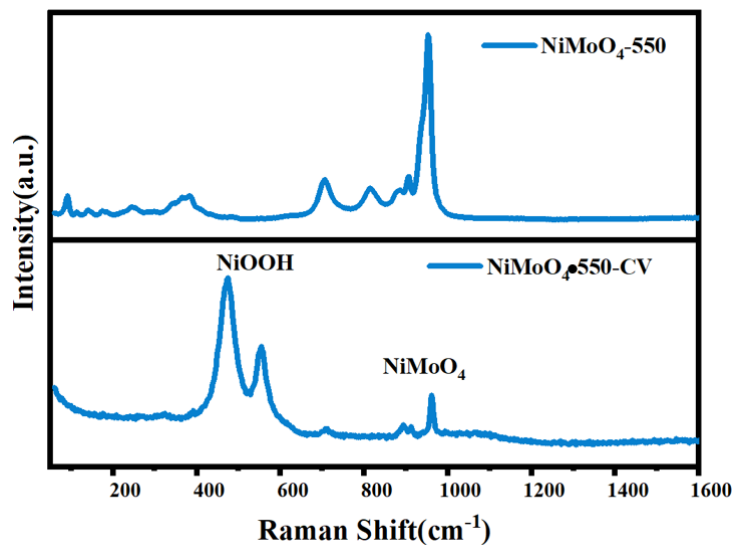
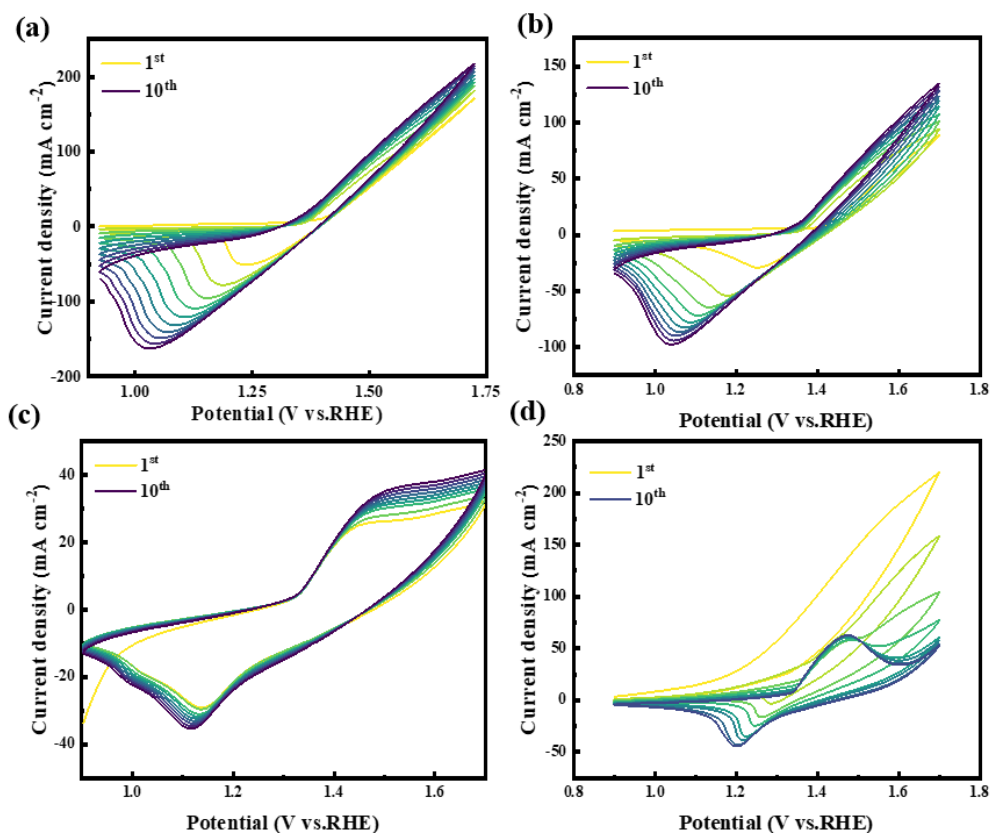Figure S6 Raman spectrum of NiMoO$_4$-550

Figure S7 Evolutive CV curves of (a)NiMoO$_4$•x H$_2$O, (b) NiMoO$_4$-550, (c) NiMoO$_4$-350, (d) NiMoO$_4$-650.
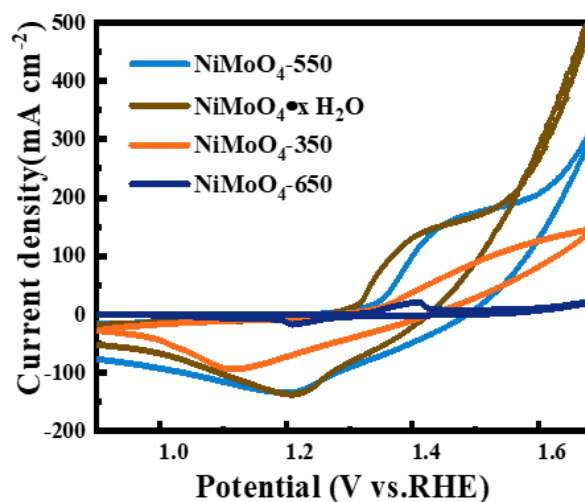
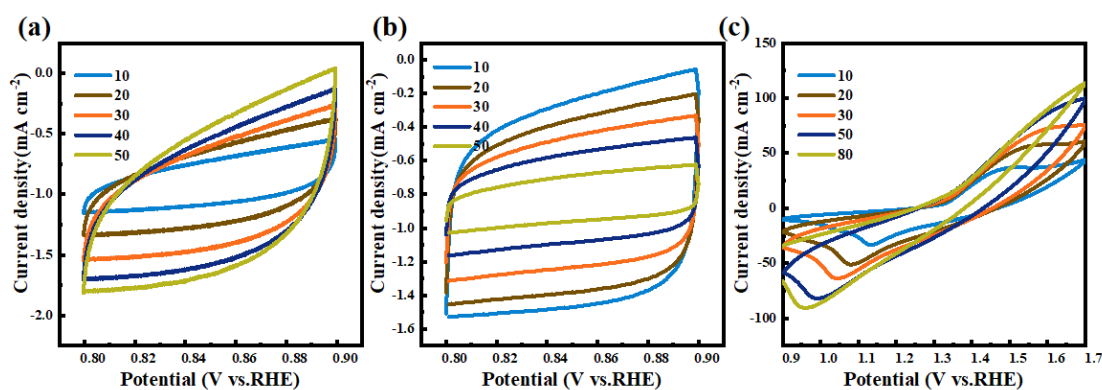Figure S8 LSV curves of samples after different heat treatments.

Figure S9 CV curves of NiMoO$_4$•xH$_2$O-CV (a) and NiMoO$_4$-550-CV (b) at the potential of 0.8-0.9 V vs. RHE (for C$_{dl}$ in Figure 3e); (c) CV curves of NiMoO$_4$-550-CV at the potential of 0.9-1.7 V vs. RHE (for the surface coverage of electroactive species (Γ∗) in Figure 4f).
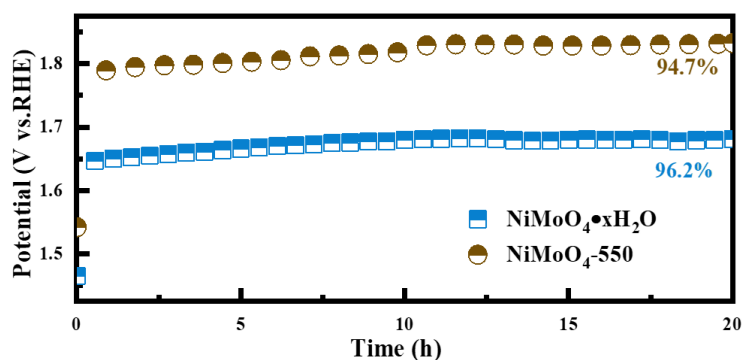

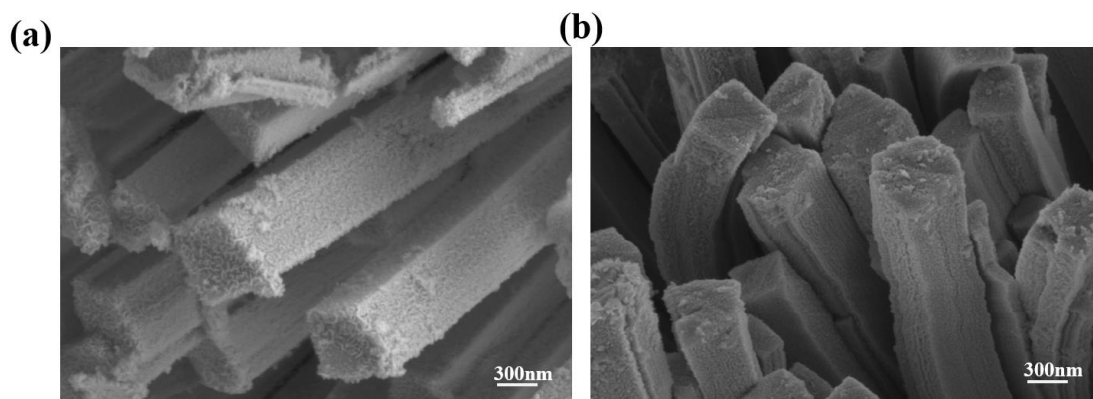Figure S10 Long-time duration test of (a) NiMoO$_4$•xH$_2$O and (b) NiMoO$_4$-550 at a current density of 100 mA cm^{-2}

(a)　　　　　　　　　　　　**(b)**

Figure S11 SEM images of (a) NiMoO$_4$•xH$_2$O and (b) NiMoO$_4$-550 after long-time duration test at a current density of 100 mA cm^{-2}.

(a)　　　　　　　　　　　　**(b)**

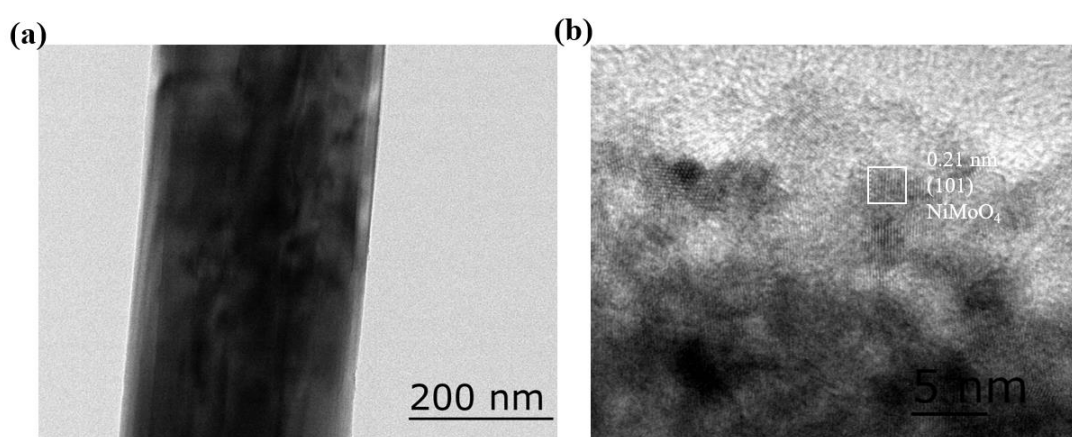
Figure S12 (a, b) TEM images of NiMoO$_4 \cdot$xH$_2$O.

Table S13 The overpotential and Tafel slope in different references

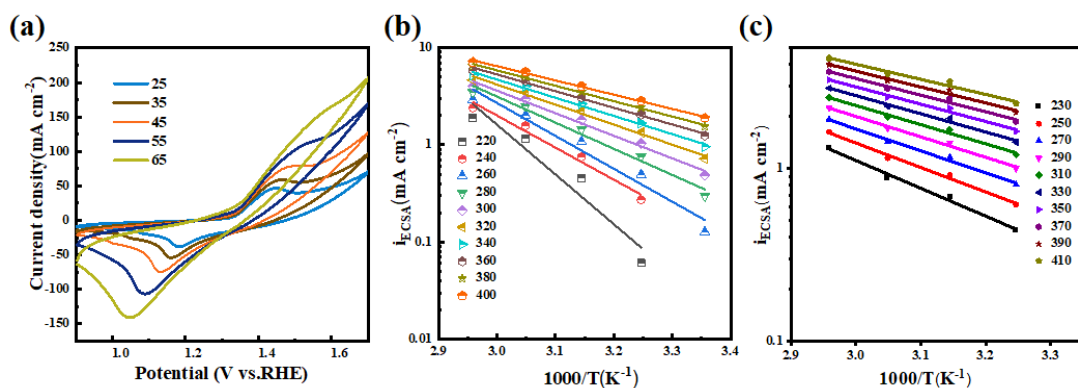|	Overpotential/mV	Tafel/mV dec^{-1}	
N-NiMoO$_4$/Ni/CNTs	330	89.5	[1]
NiMoO$_4$@Co$_3$O$_4$	120	58	[2]
NiMoO$_4$-NRs@RGO	185	54	[3]
NiMoO$_4$ nanorods	340	45.6	[4]
NiMoO$_4-x$/MoO$_2$	233	69	[5]
Fe-CQDs/NiMoO$_4$/NF	336	71.8	[6]
FeOOH-decorated NiMoO$_4$	208	60.1	[7]
NiMoO$_4$	239	71.8	[8]
NMO-30M	260	85.7	[9]
G@MoNi$_4$-NiMoO$_4$/NF	206	42	[10]
N-NiMoO$_4$/NiO$_2$	185.6	91.4	[11]
Fe-NiMoO$_4$-clusters/NF	170	54.6	[12]
NiMoO$_4$-ZIF	235	68.8	[13]

Figure S14 (a) CV curves at different temperatures of $NiMoO_4$-550-CV; The logarithm of the catalytic current density plotted against 1000 times the reciprocal of the temperature (in Kelvin) to extract the apparent activation energy (Eapp) and the pre-exponential factor (Aapp) of the OER on (b) $NiMoO_4 \cdot xH_2O$-CV and (c) $NiMoO_4$-550 catalysts at fixed overpotentials using the Arrhenius plots. The extracted E_{app} values and the pre-exponential factors (Aapp) are shown in Figure 5d, respectively.
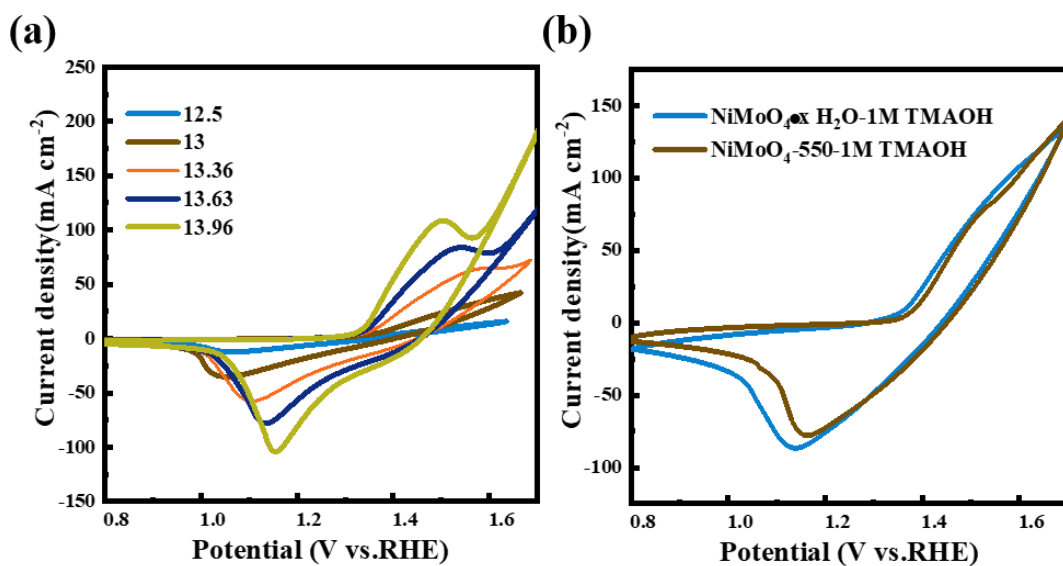

Figure S15 (a) CV curves $NiMoO_4$-550-CV under different pHs; (b) CV curves of $NiMoO_4 \cdot x$ H_2O-CV and $NiMoO_4$-550-CV in 1M TMAOH.
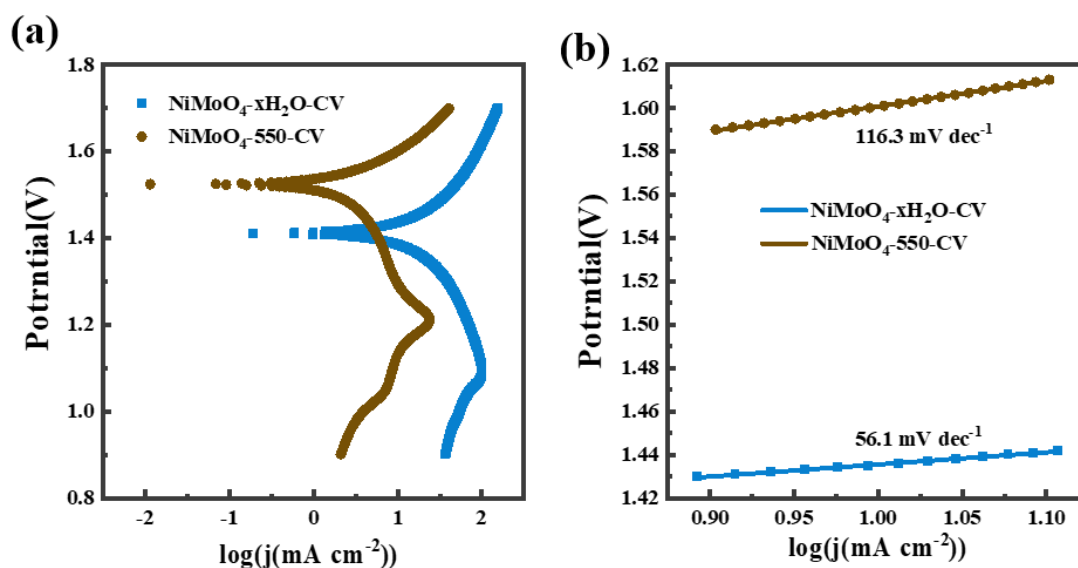
Figure S16 Tafel slope of NiMoO₄-550-CV and NiMoO₄-xH₂O-CV without iR compensation for the OER determined with steady-state measurements.

Supplementary references

1. L. An, J. Feng, Y. Zhang, R. Wang, H. Liu, G. Wang, F. Cheng and P. Xi, Epitaxial Heterogeneous Interfaces on N-NiMoO₄/NiS₂ Nanowires/Nanosheets to Boost Hydrogen and Oxygen Production for Overall Water Splitting, Adv. Funct. Mater., 2019, 29, 1, DOI: 10.1002/adfm.201805298.

2. G. Solomon, A. Landström, R. Mazzaro, M. Jugovac, P. Moras, E. Cattaruzza, V. Morandi, I. Concina and A. Vomiero, NiMoO₄@Co₃O₄ Core–Shell Nanorods: In Situ Catalyst Reconstruction toward High Efficiency Oxygen Evolution Reaction, Adv. Energy Mater., 2021, 11, 32, DOI: 10.1002/aenm.202101324.

3. G. Li, X. Qiao, Y. Miao, T. Wang and F. Deng, Synergistic Effect of N-NiMoO₄/Ni Heterogeneous Interface with Oxygen Vacancies in N-NiMoO₄/Ni/CNTs for Superior Overall Water Splitting, Small, 2023, 19, 28, DOI: 10.1002/smll.202207196.

4. V. M. Jiménez, A. Fernández, J. P. Espinós and A. R. González-Elipe, The state of the oxygen at the surface of polycrystalline cobalt oxide, J. Electron Spectrosc. Relat. Phenom., 1995, 71, 61–71, DOI: 10.1016/0368-2048(94)02238-0.

5.X. Zhao, J. Meng, Z. Yan, F. Cheng and J. Chen, Nanostructured NiMoO₄ as active electrocatalyst for oxygen evolution, Chin. Chem. Lett., 2019, 30, 2, 319–323, DOI: 10.1016/j.cclet.2018.03.035.

6. J. Ahmed, M. Alam, M. A. Majeed Khan and S. M. Alshehri, Bifunctional electro-catalytic performances of NiMoO₄-NRs@RGO nanocomposites for oxygen evolution and oxygen reduction reactions, J. King Saud Univ., Sci., 2021, 33, 2, 101317, DOI: 10.1016/j.jksus.2020.101317.

7. Z. Wang, H. Wang, S. Ji, X. Wang, P. Zhou, S. Huo, V. Linkov and R. Wang, A High Faraday Efficiency NiMoO₄ Nanosheet Array Catalyst by Adjusting the Hydrophilicity for Overall Water Splitting, Chem. – Eur. J., 2020, 26, 52, 12067–12074, DOI: 10.1002/chem.202002310.

40. H. Hao, Y. Li, Y. Wu, Z. Wang, M. Yuan, J. Miao, Z. Lv, L. Xu and B. Wei, In-situ probing the

rapid reconstruction of FeOOH-decorated $NiMoO_4$ nanowires with boosted oxygen evolution activity, Mater. Today Energy, 2022, 23, 100887, DOI: 10.1016/j.mtener.2021.100887.

8. Y. Song, W. Sha, M. Song, P. Liu, J. Tian, H. Wei, X. Hao, B. Xu, J. Guo and J. Liang, Defect engineered ultrathin $NiMoO_4$ nanomeshes as efficient and stable electrocatalysts for overall water splitting, Ceram. Int., 2021, 47, 13, 19098–19105, DOI: 10.1016/j.ceramint.2021.03.256.

9. J. Zhu, J. Qian, X. Peng, B. Xia and D. Gao, Etching-Induced Surface Reconstruction of $NiMoO_4$ for Oxygen Evolution Reaction, Nano-Micro Lett., 2023, 15, 1, 30, DOI: 10.1007/s40820-022 01011-3.

10. L. An, X. Zang, L. Ma, J. Guo, Q. Liu and X. Zhang, Graphene layer encapsulated $MoNi_4$–$NiMoO_4$ for electrocatalytic water splitting, Appl. Surf. Sci., 2020, 504, 144390, DOI: 10.1016/j.apsusc.2019.144390.

11. Z. Hou, F. Fan, Z. Wang and Y. Du, A stable N-doped $NiMoO_4$/NiO_2 electrocatalyst for efficient oxygen evolution reaction, Dalton Trans., 2024, 53, 7430–7435, DOI: 10.1039/D3DT04034H.

12. Q. Yue, R. Guo, R. Wang, G. Zhang, Y. Huang, L. Guan, W. Zhang and T. Wuren, In situ preparation of Fe-doped $NiMoO_4$ nanoflower clusters as efficient electrocatalysts for oxygen evolution reaction and overall water splitting, Electrochim. Acta, 2024, 484, 144071, DOI: 10.1016/j.electacta.2024.144071

13. M. Song, X. Lu, M. Du, Z. Chen, C. Zhu, H. Xu, W. Cheng, W. Zhuang, Z. Li, and L. Tian, Electronic and architecture engineering of hammer-shaped Ir–NiMoO4 -ZIF for effective oxygen evolution. CrystEngComm, 2022. 24, 5995–6000, DOI: 10.1039/D2CE00924B.